Heliyon 10 (2024) e35530

Contents lists available at ScienceDirect

Heliyon

journal homepage: www.cell.com/heliyon

Research article

An Auto-Reading probe system for detecting deletion mutations In liquid biopsy with direct quantification of mutation abundance

Bang Zhu [a,c,1], Jingcong Zhou [d,1], Hong He [e], Yangwei Liao [d,**], Qiaolin Li [a,b,*]

[a] Department of Gastrointestinal Surgery, The First Affiliated Hospital of Yangtze University, Jingzhou, 434023, China
[b] Digestive Disease Research Institution of Yangtze University, Clinical Medical College, Yangtze University, Jingzhou of Hubei Province, China
[c] Southern Medical University, Guangzhou, 510515, China
[d] Department of Biliary-Pancreatic Surgery, Tongji Hospital, Tongji Medical College, Huazhong University of Science and Technology, Wuhan, Hubei, 430030, China
[e] Department of Nuclear Medicine, The First Affiliated Hospital of Yangtze University, Jingzhou, 434023, China

ARTICLE INFO

Keywords:
Deletion mutation
Nucleic acid probe
DNA displacement reaction
Liquid biopsy
NIPT

ABSTRACT

Background: Deletion mutations have been confirmed to be closely related to the occurrence and progression of different hereditary diseases and tumors. Specifically, the deletion of a small number of bases is more challenging to be captured and differentiated. In non-invasive prenatal testing (NIPT) and liquid biopsy targeting circulating tumor DNA, obtaining accurate mutation abundance in targeted DNA is a crucial step in the detection process. However, the quantification of mutation abundance with existing methods is not accurate enough.
Results: Herein, we developed the " Auto-Reading" probe detection system based on our previous work. Through theoretical modeling and experimental calculations, we verified the successful application of our system in NIPT and early cancer diagnosis, enabling effective discrimination of different mutant abundances.
Significance: Our method overcomes the interference of reaction concentrations on signal detection, allowing direct quantification of mutation abundance without the need for purification of PCR products. The detection system is cost-effective and feasible for laboratory use. We believe the system will facilitate broad applications in mutation detection.

1. Introduction

With the ongoing advancements in genetic testing technology [1,2], numerous types of gene mutations have been conclusively linked to the onset and progression of diverse hereditary diseases and tumors [3–5]. Among these mutations, deletions frequently result in the misexpression or absence of one or more amino acids, exerting a profound impact on the organism [6]. For example, a four-base deletion (CTTT) in CD41/42 results in a frameshift mutation, affecting the synthesis of beta-globin and causing varying degrees of thalassemia in newborns [7]. Additionally, the deletion of exon 19 in EGFR is closely associated with the development of non-small cell lung cancer (NSCLC) and thyroid cancer [8–10]. Due to the strong correlation between deletion mutations and the occurrence and development of diseases, detection of deletion mutations is of paramount importance. Specifically, in the context of

* Corresponding author. Department of Gastrointestinal Surgery, The First Affiliated Hospital of Yangtze University, Jingzhou, 434023, China.
** Corresponding author.
E-mail addresses: 1518253446@qq.com (Y. Liao), liqiaoin@163.com (Q. Li).
[1] These authors contribute equally.

https://doi.org/10.1016/j.heliyon.2024.e35530
Received 4 July 2024; Received in revised form 24 July 2024; Accepted 30 July 2024
Available online 31 July 2024

deletion mutation detection, the deletion of a small number of bases is more challenging to be captured and differentiated with existing detection methods compared to the deletion of a big piece of DNA.

In the realm of genetic diseases, non-invasive prenatal testing (NIPT) represents a pivotal area of investigation, focusing on methods that are minimally invasive, straightforward, and applicable during early pregnancy [11,12]. Expectant mothers seeking NIPT often present with heterozygous mutations associated with autosomal recessive genetic disorders [13]. Maternal plasma DNA typically comprises a minor fraction (10%–20 %) of fetal DNA and a predominant fraction (80%–90 %) of maternal cell-free DNA [14,15], resulting in detected maternal plasma DNA genotypes typically ranging between 40 % and 60 %.Therefore, accurately determining the mutation abundance (within the 40%–60 % range) is highly necessary in NIPT. The existing NIPT technology is mainly used to detect chromosomal aneuploidy by sequencing the fetal DNA [16,17]. It is still not considered a first-line diagnostic screening method for confirmation of trisomies in pregnancies owing to the presence of false positives and false negatives [18]. Furthermore, NIPT for deletion mutations hasn't been fully studied. Moreover, in the context of early cancer screening, liquid biopsy techniques provide benefits due to their minimally invasive nature and potential for early implementation [19,20]. In liquid biopsy targeting circulating tumor DNA, the direct assessment of mutation abundance in the target DNA fragments from peripheral blood has significant implications [21]. Accurate measurement of mutation abundance in target genes aids in the early diagnosis of cancer, the staging of the middle and late stage and the evaluation of the curative effect.

Presently, prominent methodologies for quantifying deletion mutation abundance encompass high-throughput sequencing [22,23], droplet digital PCR (ddPCR) [24], and DNA probe-based methods [25,26]. Both high-throughput sequencing and ddPCR allow for absolute quantification of mutant DNA and wild-type DNA. However, these methods are expensive and time-consuming, making them unsuitable for routine use in laboratories or clinical diagnostics. DNA probe-based methods include molecular beacons (MB) probes [27], loop-mediated isothermal amplification (LAMP) [28], and graphene oxide (GO)-assisted detection [29,30], among others. MB and GO detection methods can detect various types of deletion mutations, but their lower limits of mutation abundance are only 2 % and 1 % [31], respectively, which do not meet the requirements for early cancer screening. Although the LAMP method has a lower detection limit (0.1 %), it amplifies the signals generated by mutant DNA, making it difficult to effectively differentiate mutation abundances within the range of 40 %–60 % [32]. In other words, signal amplification-based detection methods are difficult to apply to non-invasive prenatal testing (NIPT). Furthermore, all these methods necessitate the establishment of standard curves for comparison, rather than direct quantification of mutation abundance. In this scenario, the mutation abundance in the reaction mixture can be influenced by detection sensitivity. Typically, detected reaction materials originate from PCR products of genomic DNA. The inherent variability of PCR significantly impacts the accurate quantification of product concentration. Hence, precise quantification of mutation abundance using these approaches remains challenging.

In conclusion, a cost-effective and laboratory-feasible method for direct quantification of deletion mutations is currently lacking.

2. Materials and methods

2.1. Materials

ThermoPol reaction buffer was purchased from New England Biolabs (Ipswich, MA, USA). Hieff qPCR SYBR Green Master Mix (High Rox Plus) was purchased from Yeasen Biotech Co. (Shanghai, China). PCR product purification kit was purchased from Tiangen Biotech Co. (Beijing, China). DNA strands were synthesized and purified by high-performamce liquid chromatography (HPLC; Sangon Biotech Co., Shanghai, China). The sequences of all the probes and targets that have been studied in this work are summarized in Tables S1 and S2 (see Supporting Information).

2.2. Methods

2.2.1. Detection method of the auto-reading probe system

Reaction system was made up with appropriate amount of BLK1, BLK2, FAM, and BHQ, Target DNA (MT/WT) solution, ddH2O and ThermoPol reaction buffer. The total volume was 50ul. Target DNA and BLK1 or BLK2, FAM and BHQ were heated at 85 °C for 3 min, extended at 55 °C for 3 min, and then incubated at 37 °C for 30 min to form a complementary double-strand structure. Then, FAM-BHQ dsDNA were added to the system where Target DNA and BLK existed. The concentrations of FAM-BHQ, BLK, Target DNA (MT/WT) were 500 nM, 2400 nM, 200–400 nM respectively. The fluorescence was detected on a microplate reader (BioTek, American). Instrument parameters are set as follows: excitation wavelengths was 485 nm, emission wavelengths was 528 nm, and detection time was 1–2h.

2.2.2. Detection of genomic DNA after PCR

Genomic DNA was extracted from blood samples and sequenced to determine mutation points and abundance. The fragment to be detected was obtained by a two-step PCR method. The first step was a conventional PCR and the second step was the asymmetric PCR. The conventional PCR reaction system was made up with 12.5ul of PCR mix, 200 nM of forward primer, 200 nM of reversed primer, 25 ng of gDNA and H2O. Procedure: pre-denaturation at 95 °C for 1 min, denaturation at 95 °C for 15 s, annealing at 55 °C for 30 s, extension at 72 °C for 15 s, for 40 cycles. The product of the first step was diluted 100 times and be mixed to prepared the substrates with the mutation abundance of 45 %, 50 % and 55 %. These substrates were as templates for the second step of asymmetric PCR. We added 25ul of PCR mix, 1000 nM of forward primer, 100 nM of reversed primer, 1ul of the template, and H2O to make the total volume was 50ul. After two-step PCR, FAM-BHQ (500 nM), products of PCR (10 μL or 20 μL), BLK (2400 nM) were added to new tubes. Then these tubes were immediately put into a microplate reader (Biotek) for the fluorescence measurement.

3. Results and discussion

3.1. Verification of the feasibility of the " Auto-Reading" probe detection system

Based on the aforementioned analysis and building upon our previous findings [33], we have recognized the necessity to develop self-referenced probes for detecting deletion mutations in our research field. Accordingly, we devised the "Auto-Reading" probe detection system. As shown in Fig. 1a, this system consists of DNA strands named as BLK1, BLK2, FAM, and BHQ. FAM and BHQ have complementary regions and are labeled with “FAM” and “BHQ”. BLK1 is a perfect match with the wild type DNA (WT) and has a few mismatches with the mutant type DNA (MT), resulting in a bubble formation in BLK1. Similarly, BLK2 is a perfect match with MT and has a few mismatches with WT, causing a bubble formation in WT. MT and WT can partially hybridize with FAM to different extents. When MT and WT, pre-mixed with BLK1 (Target group) or BLK2 (Reference group), are added to the reaction system within FAM-BHQ dsDNA, four different reactions occur:

$$BLK1-MT+FAM-BHQ \rightleftharpoons FAM-MT+BLK1-BHQ \quad \Delta G_1<0 \tag{1}$$

$$BLK1-WT+FAM-BHQ \rightleftharpoons FAM-WT+BLK1-BHQ \quad \Delta G_2>0 \tag{2}$$

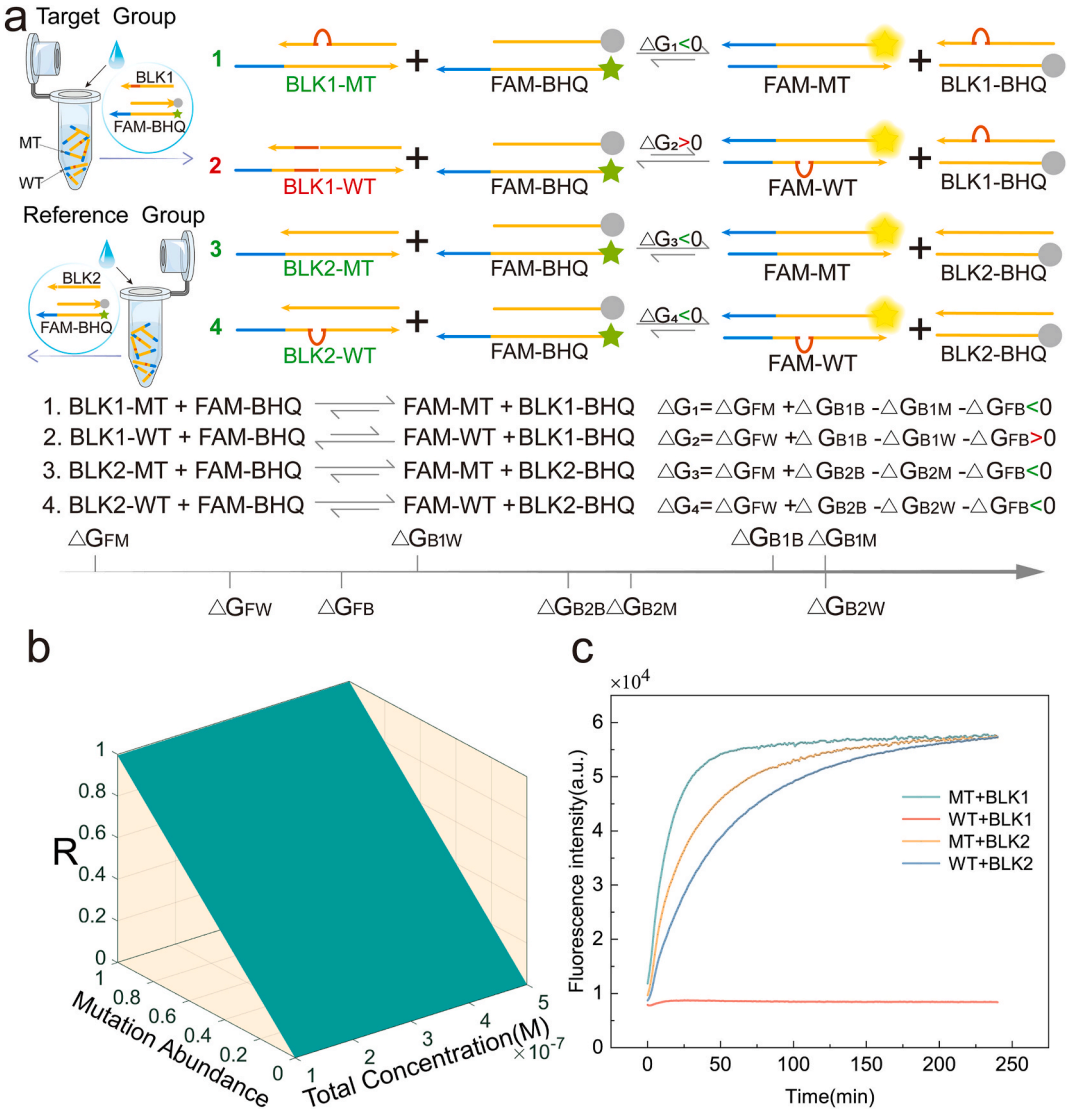

Fig. 1. (a) The Schematic Illustration of the " Auto-Reading" probe detection system. (b) Three-dimensional graph shows the relation of mutation abundance, total concentration and the calculated signal ratio R. It illustrates that 1−R and r remain linear when C changes. (c) The curve of fluorescence changing over time of the four reactions.

$$BLK2-MT+FAM-BHQ\rightleftharpoons FAM-MT+BLK2-BHQ \quad \Delta G_3<0 \tag{3}$$

$$BLK2-WT+FAM-BHQ\rightleftharpoons FAM-WT+BLK2-BHQ \quad \Delta G_4<0 \tag{4}$$

The thermodynamic calculations for these reactions are depicted above. It is noted that G1 = G3 = G4 < 0, while G2 > 0. In reactions 1, 3, and 4, no more bubble which brings the thermodynamic differences forms, and the reactions are essentially at equilibrium. However, reaction 2 has two extra bubbles in the product compared to the reactant, which significantly affects the stability of the product. Therefore, reaction 2 is difficult to proceed in the forward direction. We designed the sequences corresponding to these strands, centered around the CD41-42 deletion mutation site, and predicted the thermodynamic values for the four reactions using NUPACK (see the supplementary materials for details), which were consistent with our expectations. Next, we constructed a model for calculating substrate mutation abundance:

$$BLK1+MT\rightleftharpoons BLK1-MT \quad \Delta G_5<0 \tag{5}$$

$$e^{-\frac{\Delta G5}{RT}}=\frac{x_1}{([BLK1]-x_1)([MT]-x_1)} \tag{6}$$

In equation (6), [BLK1] is the initial concentration of BLK1, [MT] is the initial concentration of MT, and x_1 is the equilibrium concentration of BLK1-MT.

$$BLK1+WT\rightleftharpoons BLK1-WT \quad \Delta G_6<0 \tag{7}$$

$$BLK2+MT\rightleftharpoons BLK2-MT \quad \Delta G_7<0 \tag{8}$$

$$BLK2+WT\rightleftharpoons BLK2-WT \quad \Delta G_8<0 \tag{9}$$

Similarly, the following equation can be obtained from the thermodynamics of reaction (6)(7) and (8):

$$e^{-\frac{\Delta G6}{RT}}=\frac{x_2}{([BLK1]-x_2)([WT]-x_2)} \tag{10}$$

$$e^{-\frac{\Delta G7}{RT}}=\frac{x_3}{([BLK2]-x_3)([MT]-x_3)} \tag{11}$$

$$e^{-\frac{\Delta G8}{RT}}=\frac{x_4}{([BLK2]-x_4)([WT]-x_4)} \tag{12}$$

The following equation can be obtained from the thermodynamics of reaction (1):

$$e^{-\frac{\Delta G1}{RT}}=\frac{a1^2x_1}{(P_0-a_1x_1)(1-a_1)} \tag{13}$$

In equation (13), a_1x_1 is the concentration of $FAM-MT$ and $1-BHQ$, P_0 is the initial concentration of FAM-BHQ. Similarly, the following equation can be obtained from the thermodynamics of reaction (2)(3) and (4):

$$e^{-\frac{\Delta G2}{RT}}=\frac{a2^2x_2}{(P_0-a_2x_2)(1-a_2)} \tag{14}$$

$$e^{-\frac{\Delta G3}{RT}}=\frac{a3^2x_3}{(P_0-a_3x_3)(1-a_3)} \tag{15}$$

$$e^{-\frac{\Delta G4}{RT}}=\frac{a4^2x_4}{(P_0-a_4x_4)(1-a_4)} \tag{16}$$

Then we calculated the signal ratio R between target group and reference group,

$$R=\frac{a_1x_1F_0+a_2x_2F_0}{a_3x_3F_0+a_4x_4F_0}=\frac{a_1x_1+a_2x_2}{a_3x_3+a_4x_4} \tag{17}$$

F_0 is the fluorescent signal produced by 1mol of FAM-BHQ.

Using computations and simulations in Maple, we generated the relationship graph depicting R in relation to initial mutation abundance and reactant concentration. As shown in Fig. 1b, R is not correlated with concentration but is directly proportional to the initial mutation abundance, with a proportionality coefficient of approximately 1. This means that R can effectively represent the initial mutation abundance. Therefore, we have theoretically demonstrated that this method can directly quantify the abundance of the deletion mutation. Following theoretical confirmation, experimental validation of our method was pursued. We synthesized a series of reactant DNA chains and conducted separate reactions using MT and WT variants with two distinct probes. The results shown in Fig. 1c confirmed the core principle: ΔG1 = ΔG3 = ΔG4 < 0, and ΔG2 > 0. Reaction 1, 3, and 4 occurred at similar levels, while

reaction 2 barely occurred. It should be noted that the reaction rates for reactions 1, 3, and 4 were not the same, which could be related to the distance between the bubbles and the toe region. However, the reaction rates do not affect our quantitative determination of mutation abundance. Therefore, the experimental results validated the core principle.

3.2. Simulation of the application of the " Auto-reading" probe detection system in NIPT

Subsequently, our objective was to validate the system's capability to accurately discriminate between MT and WT alleles mixed in a 1:1 ratio. In the context of non-invasive prenatal testing (NIPT), scenarios frequently arise involving heterozygous maternal gene mutations. Assuming that the proportion of cell-free fetal DNA in the maternal plasma is 10 %, the genotype of the fetal DNA could be wild-type, heterozygous, or mutant, resulting in mutant abundances of 45 %, 50 %, or 55 %, respectively. Therefore, it is necessary to accurately read and distinguish these proportions. We prepared reaction substrates with mutant abundances of 45 %, 50 %, and 55 % by synthesizing MT and WT strands mixed in ratios of 9:11, 1:1, and 11:9, respectively. Two reaction systems were designed, both incorporating probes: the target system with BLK1 and the reference system with BLK2. In addition, reaction substrates with concentrations of 200 nM and 400 nM were detected respectively. The results of the reactions are shown in Fig. 2a and b. To eliminate the interference of background signals, a negative control group without substrate was included. Thus, the calculated experimental values, $R_{45\ \%}$, $R_{50\ \%}$ and $R_{55\ \%}$ are defined as follows:

$$R_{45\%}=\frac{S_{45\%}^{BLK1}-S_{NC}}{S_{45\%}^{BLK2}-S_{NC}}, R_{50\%}=\frac{S_{50\%}^{BLK1}-S_{NC}}{S_{50\%}^{BLK2}-S_{NC}}\ , R_{55\%}=\frac{S_{55\%}^{BLK1}-S_{NC}}{S_{55\%}^{BLK2}-S_{NC}}$$

Here, $S_{45\%}^{BLK1}$ denotes the signal plateau value in the target system with 45 % mutant substrate abundance, while $S_{45\%}^{BLK2}$ represents the signal plateau value in the reference system under the same substrate conditions. Other symbols hold analogous significance. $R_{45\ \%}$, $R_{50\ \%}$ and $R_{55\ \%}$ represent the calculated mutant abundances at substrate mutant abundance of 45 %, 50 % and 55 %, respectively. By comparing the calculated values with the initial mutant abundances in Fig. 2c, we observed that our calculated R values accurately quantified the mutant abundances and were independent of the initial substrate concentrations. Furthermore, the experimental calculated R values matched the theoretical values, validating the correctness of our theoretical modeling.

3.3. Application of our method to PCR products without purification and quantification

Following validation of the theory with synthetic strands, we endeavored to illustrate the applicability of our method to PCR products without the need for purification and precise quantification. PCR products typically harbor higher levels of byproducts compared to synthetic strands, posing challenges for accurate quantification. This scenario is closer to the actual situation of PCR products obtained from purified cell-free fetal DNA in plasma samples. Therefore, we synthesized a series of long MT and WT strands, mixed them in different ratios to prepare reaction substrates with mutant abundances of 45 %, 50 %, and 55 %, and performed asymmetric PCR followed by detection using the self-reading probe system. The detection results are shown in Fig. 3a–c, indicating that the reaction system can distinguish the mutant abundances in PCR products without purification and quantification. In other words, our method has great potential for application in NIPT scenarios targeting deletion mutations.

3.4. Simulation of the application of the system in early diagnosis of cancer

To further explore the potential application of our method in the early diagnosis of cancer-related deletion mutations, we concentrated on a specific mutation, namely the BRCA1 deletion, known for its significant association with breast cancer [34]. In early

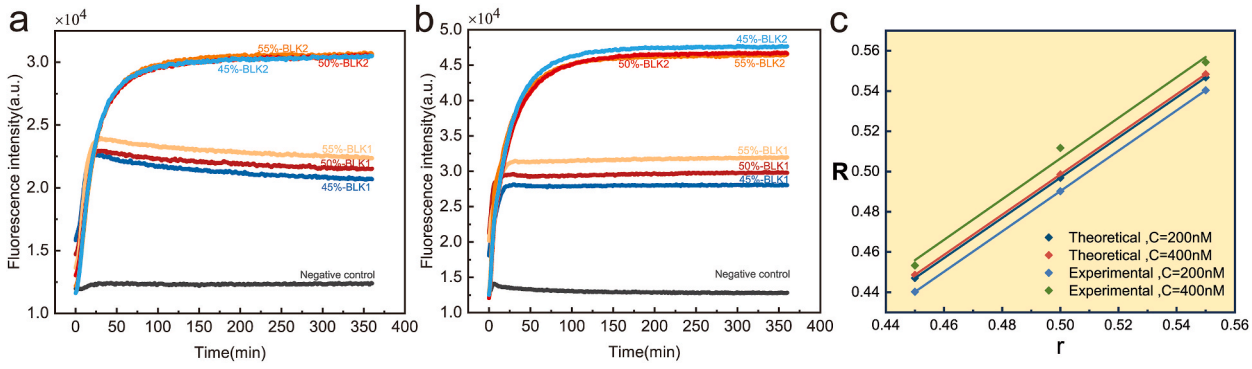

Fig. 2. (a) The reaction curve of fluorescence of substrates with mutation abundances of 45 %, 50 %, 55 % and concentrations of 200 nM. (b) The reaction curve of fluorescence of substrates with mutation abundances of 45 %, 50 %, 55 % and concentrations of 400 nM. (c) The calculated R values accurately quantified the mutant abundances and were independent of the initial substrate concentrations. Furthermore, the experimental calculated R values matched the theoretical values.

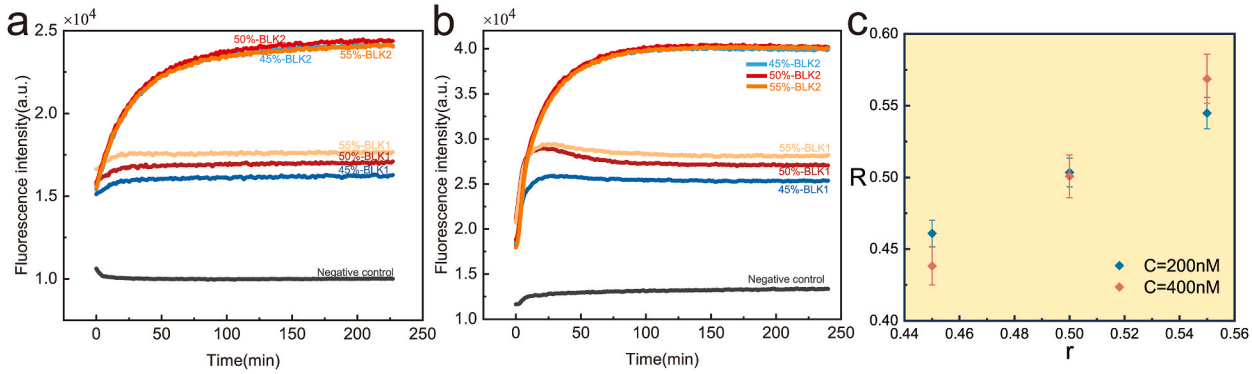

Fig. 3. (a) The reaction curve of fluorescence of PCR products with mutation abundances of 45 %, 50 %, 55 % and concentrations of 200 nM. (b) The reaction curve of fluorescence of PCR products with mutation abundances of 45 %, 50 %, 55 % and concentrations of 400 nM. (c) There is a linear relationship between calculated R values and mutation abundances.

cancer diagnosis, MT is often present in a small proportion within a large amount of WT, possibly as low as 5 % or even lower. We aimed to distinguish extremely low mutant abundances of 10 %, 5 %, 2 %, and 0 %. Accordingly, we designed and synthesized the corresponding MT, WT, BLK1, BLK2, and probe strands centered around this mutation. Firstly, through computations and simulations in Maple, we obtained the relationship graph between R and the initial mutation abundance and reactant concentration with the new DNA sequences. As shown in Fig. 4a, R is not correlated with concentration but is directly proportional to the initial mutation

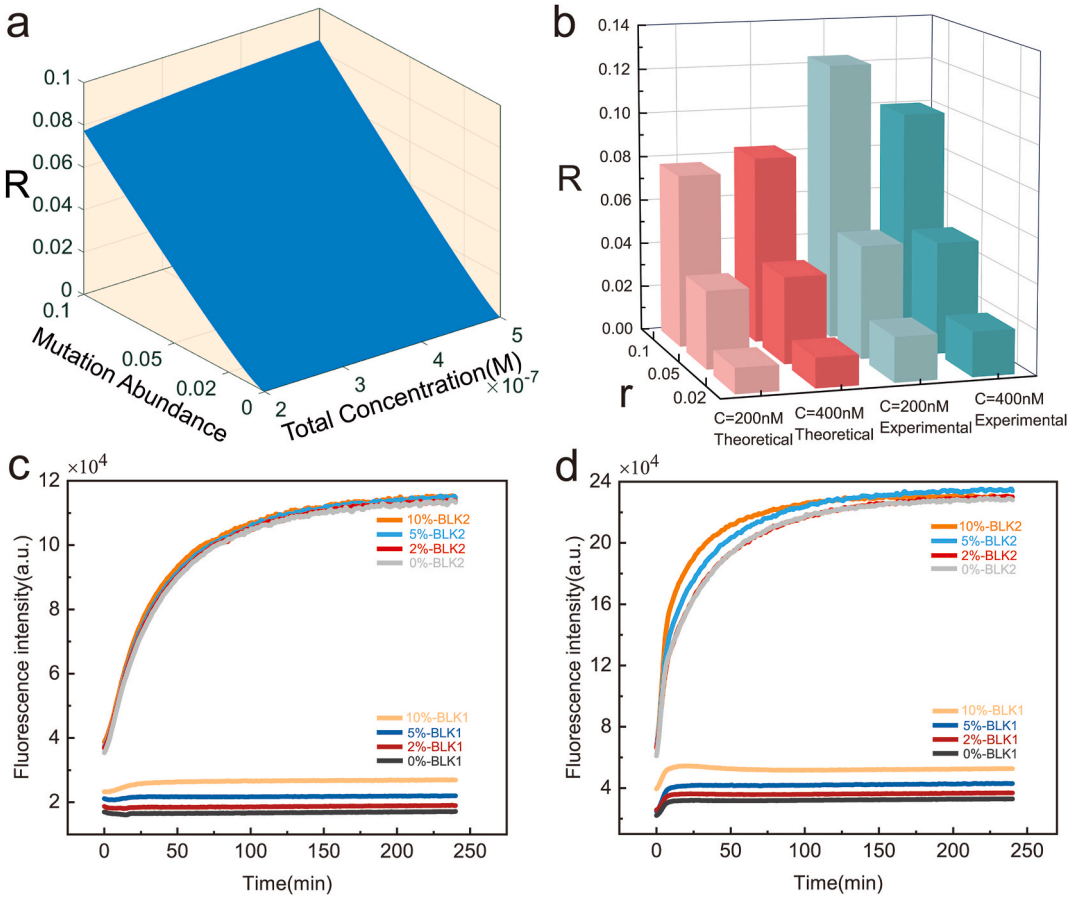

Fig. 4. (a) Three-dimensional graph shows the relation of mutation abundance of 0–0.1, total concentration and the calculated signal ratio R. (b) The calculated R values accurately quantified the mutant abundances of 0–0.1. The experimental calculated R values matched the theoretical values. (c) The reaction curve of fluorescence of substrates with mutation abundances of 0 %, 2 %, 5 %, 10 % and concentrations of 200 nM. (d) The reaction curve of fluorescence of substrates with mutation abundances of 0 %, 2 %, 5 %, 10 % and concentrations of 400 nM.

abundance of 0%–10 %. This means that R can also effectively represent the initial mutation abundance of 0%–10 %. Therefore, we have theoretically demonstrated that this method can directly quantify the abundance of the deletion mutation in early cancer diagnosis. After that, we prepared reaction substrates with mutant abundances of 10 %, 5 %, 2 %, and 0 % by mixing MT and WT in ratios of 1:9, 1:19, 1:49, respectively. The detection was performed using the self-reading probe system at different concentrations (200 nM and 400 nM). Similarly, we performed comprehensive calculations by regarding the 0 % group as control to remove the interference of background signals and obtained the following results:

$$R_{10\%}=\frac{S_{10\%}^{BLK1}-S_{0\%}^{BLK1}}{S_{10\%}^{BLK2}-S_{0\%}^{BLK1}}, R_{5\%}=\frac{S_{5\%}^{BLK1}-S_{0\%}^{BLK1}}{S_{5\%}^{BLK2}-S_{0\%}^{BLK1}}\ ,\ R_{2\%}=\frac{S_{2\%}^{BLK1}-S_{0\%}^{BLK1}}{S_{2\%}^{BLK2}-S_{0\%}^{BLK1}}$$

In the given expression, $S_{10\%}^{BLK1}$ denotes the signal plateau value observed in the target system with a mutant substrate abundance of 10 %, while $S_{10\%}^{BLK2}$ signifies the signal plateau value in the reference system under the same substrate conditions. The remaining symbols carry analogous definitions. $R_{10\ \%}$, $R_{5\%}$ and $R_{2\%}$ represent the calculated mutant abundances at substrate mutant abundance of 10 %, 5 % and 2 %, respectively. The reaction and calculation results are shown in Fig. 4b–d, revealing significant differences in the ratios of reaction substrates with mutant abundances of 2 %, 5 %, and 10 %. Importantly, these ratios remained consistent regardless of the substrate quantity. Additionally, the experimentally calculated R values matched the theoretically predicted R values. Therefore, we have demonstrated that our method can detect mutant abundances as low as 2 %.

3.5. *Clinical applications of our method in early diagnosis of cancer*

Furthermore, we aimed to investigate the clinical applicability of our method. As illustrated in Fig. 5a, blood samples were

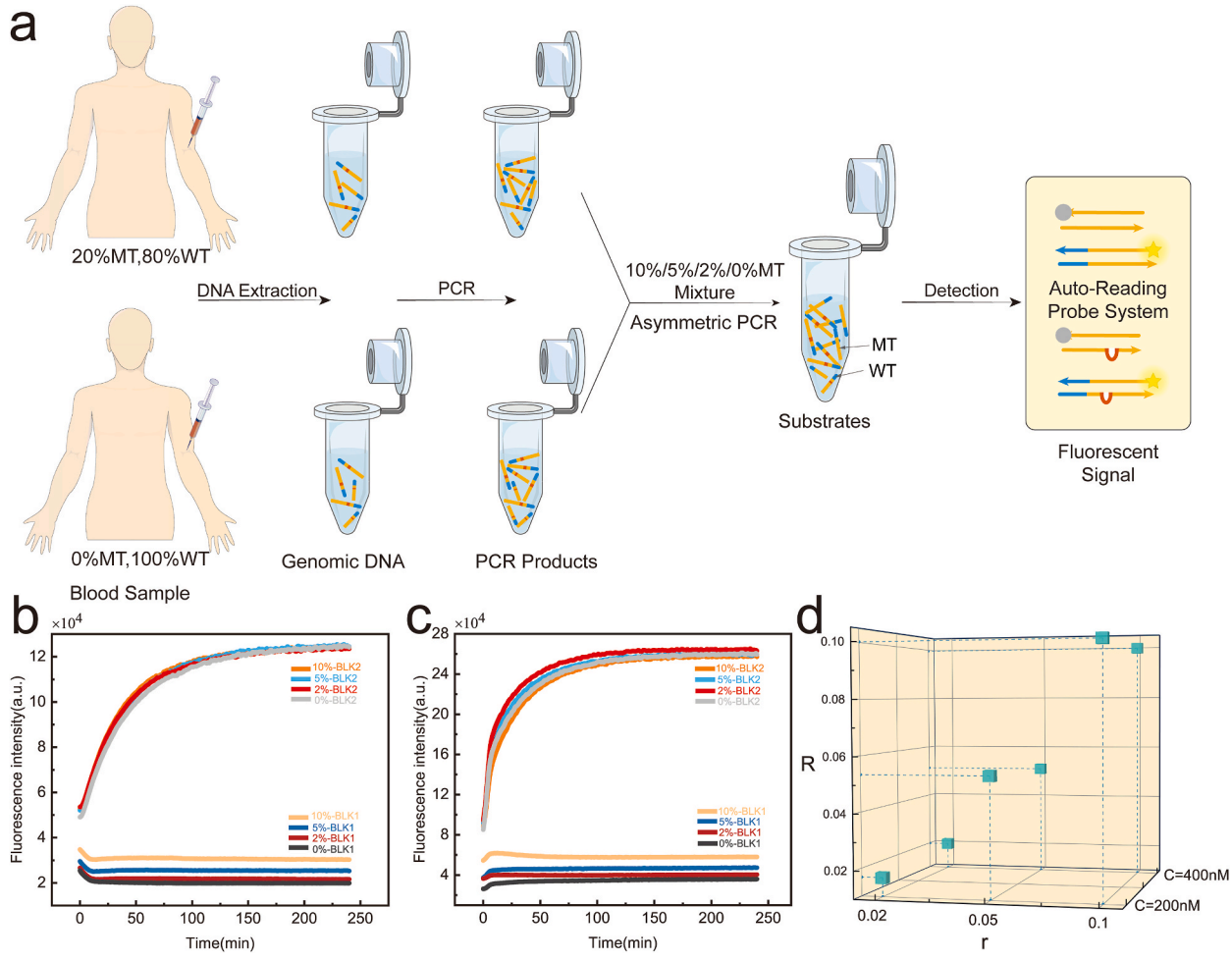

Fig. 5. (a) The Schematic Illustration of the procedure of the clinical applications. (b) The reaction curve of fluorescence of PCR products with mutation abundances of 0 %, 2 %, 5 %, 10 % and volumes of 10ul. (c) The reaction curve of fluorescence of PCR products with mutation abundances of 0 %, 2 %, 5 %, 10 % and volumes of 20ul. (d) Three-dimensional graph shows the relation of mutation abundance r, total concentration and the calculated signal ratio R. The experimental calculated R values matched the theoretical values in both concentrations.

collected exhibiting mutation abundances of 20 % and 0 %.After purifying the asymmetric PCR products and quantifying their concentrations, we prepared reaction substrates with mutant abundances of 0 %, 2 %, 5 %, and 10 % by adjusting the ratios of the purified products. The detection was performed using asymmetric PCR followed by the self-reading probe system. The detection results, as shown in Fig. 5b–d, indicate that the detection system can differentiate these reaction substrates. This further supports the potential application of our method in the early diagnosis of tumors. Due to the complexity of the reaction system, we cannot distinguish the mutation abundance between 2% and 0% of the reaction substrates at present. However, comparing with the above methods, our method allows for direct quantification of mutation abundance.

4. Conclusion

In this work, we developed an Auto-Reading Probe System targeting the detection of multi-base deletion mutations and innovatively applied the concept of self-reference in the context of deletion mutation detection. The challenge in designing self-referencing for multi-base deletion mutations stems from the inability to adjust for thermodynamic differences using a gapped probe, a limitation also recognized in single-base substitution mutations. In our design, we directly utilize the bubble structure as a means to balance thermodynamic differences. Fortunately, this thermodynamic variation does not disrupt reaction kinetics within a manageable range nor perturb the equilibrium of our reaction system. Through theoretical modeling and experimental calculations, we have verified the successful application of our system in NIPT and early cancer diagnosis, enabling effective discrimination of different mutant abundances. Our method circumvents the impact of reaction concentrations on signal detection, enabling direct quantification of mutant abundances without the necessity of PCR product quantification. Therefore, our method proves to be cost-effective and practical for laboratory applications. We anticipate that our method will foster extensive applications in mutation detection, including its utility in guiding the optimization and deployment of enzyme-based amplification and PCR-based detection methods through theoretical models.

Research Funding

This project has practical values and is supported by Nature Science Foundation of Hubei Province (2023AFB969), the Doctoral Starting up Foundation of The First Affiliated Hospital of Yangtze University (2022DIF04), China, and the Fundamental Research Funds for the Central Universities (YCJJ20230236).

Ethics approval and consent to participate

This study was approved by the Institutional Ethics Committee of Tongji Hospital, Huazhong University of Science and Technology (approval no. TJ-IRB20190418), and abided by the principles of the Declaration of Helsinki. The informed consent was obtained from all the participants in accordance with the national legislation and the Declaration of Helsinki.

Data availability statement

Data used and/or analyzed in the current study are available from the corresponding author upon reasonable request.

CRediT authorship contribution statement

Bang Zhu: Writing – original draft, Methodology, Conceptualization. **Jingcong Zhou:** Visualization, Validation, Data curation. **Hong He:** Resources, Data curation. **Yangwei Liao:** Writing – original draft, Funding acquisition, Conceptualization. **Qiaolin Li:** Writing – review & editing, Funding acquisition.

Declaration of competing interest

The authors declare that they have no known competing financial interests or personal relationships that could have appeared to influence the work reported in this paper.

Appendix A. Supplementary data

Supplementary data to this article can be found online at https://doi.org/10.1016/j.heliyon.2024.e35530.

References

[1] S.X. Chen, D.Y. Zhang, G. Seelig, Conditionally fluorescent molecular probes for detecting single base changes in double-stranded DNA, Nat. Chem. 5 (2013) 782–789, https://doi.org/10.1038/nchem.1713.

[2] F. Li, J. Li, W. Yang, S. Yang, C. Chen, L. Du, .P. Liu, Framework-hotspot enhanced trans cleavage of CRISPR-cas12a for clinical samples detection, Angew Chem. Int. Ed. Engl. 62 (2023) e202305536, https://doi.org/10.1002/anie.202305536.

[3] T.R. Rebbeck, N. Mitra, F. Wan, O.M. Sinilnikova, S. Healey, L. McGuffog, .I. Andrulis, Association of type and location of BRCA1 and BRCA2 mutations with risk of breast and ovarian cancer, JAMA 313 (2015) 1347–1361, https://doi.org/10.1001/jama.2014.5985.

[4] E.N. Bergstrom, J. Luebeck, M. Petljak, A. Khandekar, M. Barnes, T. Zhang, L.B. Alexandrov, Mapping clustered mutations in cancer reveals APOBEC3 mutagenesis of ecDNA, Nature 602 (2022) 510–517, https://doi.org/10.1038/s41586-022-04398-6.

[5] Q. Zhou, X.C. Zhang, Z.H. Chen, X.L. Yin, J.J. Yang, C.R. Xu, .Y.L. Wu, Relative abundance of EGFR mutations predicts benefit from gefitinib treatment for advanced non-small-cell lung cancer, J. Clin. Oncol. 29 (2011) 3316–3321, https://doi.org/10.1200/JCO.2010.33.3757.

[6] E. Nolan, G.J. Lindeman, J.E. Visvader, Out-RANKing BRCA1 in mutation carriers, Cancer Res. 77 (2017) 595–600, https://doi.org/10.1158/0008-5472.CAN-16-2025.

[7] D.P. Dever, R.O. Bak, A. Reinisch, J. Camarena, G. Washington, C.E. Nicolas, M.H. Porteus, CRISPR/Cas9 beta-globin gene targeting in human haematopoietic stem cells, Nature 539 (2016) 384–389, https://doi.org/10.1038/nature20134.

[8] Y.H. Teng, W.J. Tan, A.A. Thike, P.Y. Cheok, G.M. Tse, N.S. Wong, .P.H. Tan, Mutations in the epidermal growth factor receptor (EGFR) gene in triple negative breast cancer: possible implications for targeted therapy, Breast Cancer Res. 13 (2011) R35, https://doi.org/10.1186/bcr2857.

[9] L. Hu, D. Shen, D. Liang, J. Shi, C. Song, K. Jiang, .S. Meng, Thyroid receptor-interacting protein 13 and EGFR form a feedforward loop promoting glioblastoma growth, Cancer Lett. 493 (2020) 156–166, https://doi.org/10.1016/j.canlet.2020.08.023.

[10] E. Castellanos, E. Feld, L. Horn, Driven by mutations: the predictive value of mutation subtype in EGFR-mutated non-small cell lung cancer, J. Thorac. Oncol. 12 (2017) 612–623.

[11] P. Benn, H. Cuckle, E. Pergament, Non-invasive prenatal testing for aneuploidy: current status and future prospects, Ultrasound Obstet. Gynecol. 42 (2013) 15–33.

[12] R.W. Chiu, Y.M. Lo, C.T. Wittwer, Molecular diagnostics: a revolution in progress, Clin. Chem. 61 (2015) 1–3.

[13] I. Hudecova, R.W. Chiu, Non-invasive prenatal diagnosis of thalassemias using maternal plasma cell free DNA, Best Pract. Res. Clin. Obstet. Gynaecol. 39 (2017) 63–73.

[14] Y.M. Lo, K.C. Chan, H. Sun, E.Z. Chen, P. Jiang, F.M. Lun, .R.W. Chiu, Maternal plasma DNA sequencing reveals the genome-wide genetic and mutational profile of the fetus, Sci. Transl. Med. 2 (2010) 61ra91, https://doi.org/10.1126/scitranslmed.3001720.

[15] K.C. Chan, J. Zhang, A.B. Hui, N. Wong, T.K. Lau, T.N. Leung, .Y.M. Lo, Size distributions of maternal and fetal DNA in maternal plasma, Clin. Chem. 50 (2004) 88–92.

[16] Y. Liu, H. Liu, Y. He, W. Xu, Q. Ma, Y. He, .F. Yu, Clinical performance of non-invasive prenatal served as a first-tier screening test for trisomy 21, 18, 13 and sex chromosome aneuploidy in a pilot city in China, Hum Genomics 14 (2020) 21, https://doi.org/10.1186/s40246-020-00268-2.

[17] J. Jin, J. Yang, Y. Chen, J. Huang, Systematic review and meta-analysis of non-invasive prenatal DNA testing for trisomy 21: implications for implementation in China, Prenat. Diagn. 37 (2017) 864–873, https://doi.org/10.1002/pd.5111.

[18] P. Brady, N. Brison, K. Van Den Bogaert, T. de Ravel, H. Peeters, H. Van Esch, .J.R. Vermeesch, Clinical implementation of NIPT - technical and biological challenges, Clin. Genet. 89 (2016) 523–530, https://doi.org/10.1111/cge.12598.

[19] M. Nikanjam, S. Kato, R. Kurzrock, Liquid biopsy: current technology and clinical applications, J. Hematol. Oncol. 15 (2022) 131.

[20] W. Li, J.B. Liu, L.K. Hou, F. Yu, J. Zhang, W. Wu, .D. Fu, Liquid biopsy in lung cancer: significance in diagnostics, prediction, and treatment monitoring, Mol. Cancer 21 (2022) 25, https://doi.org/10.1186/s12943-022-01505-z.

[21] W. Chen, H.Q. Xu, S.B. Dai, J.Y. Wang, Z.Y. Yang, Y.W. Jin, M.P. Zhao, Detection of low-frequency mutations in clinical samples by increasing mutation abundance via the excision of wild-type sequences, Nat. Biomed. Eng. 7 (2023), 1602-+.

[22] J.M. Churko, G.L. Mantalas, M.P. Snyder, J.C. Wu, Overview of high throughput sequencing technologies to elucidate molecular pathways in cardiovascular diseases, Circ. Res. 112 (2013) 1613–1623, https://doi.org/10.1161/CIRCRESAHA.113.300939.

[23] M. David, H. Mustafa, M. Brudno, Detecting Alu insertions from high-throughput sequencing data, Nucleic Acids Res. 41 (2013) e169, https://doi.org/10.1093/nar/gkt612.

[24] T. Suo, X. Liu, J. Feng, M. Guo, W. Hu, D. Guo, .Y. Chen, ddPCR: a more accurate tool for SARS-CoV-2 detection in low viral load specimens, Emerg Microbes Infect 9 (2020) 1259–1268, https://doi.org/10.1080/22221751.2020.1772678.

[25] Y. Xiao, K.J. Plakos, X. Lou, R.J. White, J. Qian, K.W. Plaxco, H.T. Soh, Fluorescence detection of single-nucleotide polymorphisms with a single, self-complementary, triple-stem DNA probe, Angew Chem. Int. Ed. Engl. 48 (2009) 4354–4358, https://doi.org/10.1002/anie.200900369.

[26] X. Xiao, T. Wu, L. Xu, W. Chen, M. Zhao, A branch-migration based fluorescent probe for straightforward, sensitive and specific discrimination of DNA mutations, Nucleic Acids Res. 45 (2017) e90, https://doi.org/10.1093/nar/gkx117.

[27] J. Zheng, R. Yang, M. Shi, C. Wu, X. Fang, Y. Li, .W. Tan, Rationally designed molecular beacons for bioanalytical and biomedical applications, Chem. Soc. Rev. 44 (2015) 3036–3055, https://doi.org/10.1039/c5cs00020c.

[28] Z. Lin, Y. Zhang, H. Zhang, Y. Zhou, J. Cao, J. Zhou, Comparison of loop-mediated isothermal amplification (LAMP) and real-time PCR method targeting a 529-bp repeat element for diagnosis of toxoplasmosis, Vet. Parasitol. 185 (2012) 296–300, https://doi.org/10.1016/j.vetpar.2011.10.016.

[29] K. Yang, L. Feng, X. Shi, Z. Liu, Nano-graphene in biomedicine: theranostic applications, Chem. Soc. Rev. 42 (2013) 530–547.

[30] F. Li, J. Chao, Z. Li, S. Xing, S. Su, X. Li, .L. Wang, Graphene oxide-assisted nucleic acids assays using conjugated polyelectrolytes-based fluorescent signal transduction, Anal. Chem. 87 (2015) 3877–3883.

[31] J. Xu, L. Li, N. Chen, Y. She, S. Wang, N. Liu, X. Xiao, Endonuclease IV based competitive DNA probe assay for differentiation of low-abundance point mutations by discriminating stable single-base mismatches, Chem. Commun. 53 (2017) 9422–9425, https://doi.org/10.1039/c7cc04816e.

[32] G. Wang, Y. Shang, Y. Wang, H. Tian, X. Liu, Comparison of a loop-mediated isothermal amplification for orf virus with quantitative real-time PCR, Virol. J. 10 (2013) 138.

[33] X. Tang, X. Chen, Y. Liao, B. Yan, H. Hu, Z. Ming, .X. Xiao, Self-internal-reference probe system for control-free quantification of mutation abundance, Anal. Chem. 93 (2021) 13274–13283, https://doi.org/10.1021/acs.analchem.1c02877.

[34] T. Akin Duman, F.N. Ozturk, Frequency and distribution of BRCA1/BRCA2 large genomic rearrangements in Turkish population with breast cancer, J. Hum. Genet. 68 (2023) 485–490, https://doi.org/10.1038/s10038-023-01140-6.